Available online at www.sciencedirect.com
SCIENCE DIRECT
Journal of Colloid and Interface Science 291 (2005) 126–134
JOURNAL OF Colloid and Interface Science
www.elsevier.com/locate/jcis

Monodisperse DNA restriction fragments II. Sedimentation velocity and equilibrium experiments

Gijsberta H. Koenderink [a], Karel L. Planken [b], Ramon Roozendaal [c,1], Albert P. Philipse [b,*]

[a] *Experimental Soft Condensed Matter Group, Division of Engineering and Applied Sciences, Harvard University, 9 & 15 Oxford Street, Cambridge, MA 02138, USA*

[b] *Van't Hoff Laboratory for Physical and Colloid Chemistry, Debye Institute, Utrecht University, Padualaan 8, 3584 CH Utrecht, The Netherlands*

[c] *MGC—Human and Clinical Genetics, Leiden University Medical Center, Wassenaarseweg 72, 2333 AL Leiden, The Netherlands*

Received 7 October 2004; accepted 29 April 2005

Available online 1 July 2005

Abstract

We report sedimentation velocity and equilibrium measurements performed with an analytical ultracentrifuge to elucidate the effects of limited flexibility on the transport properties of semiflexible, monodisperse, double-stranded, blunt-ended DNA restriction fragments. We study a homologous series of fragments with 400, 800, and 1600 base pairs (3 to 11 persistence lengths), which are specifically designed and synthesized for this purpose (Part I). The molecular weights following from the sedimentation measurements agree well with the values expected on the basis of the number of base pairs. The sedimentation coefficients at infinite dilution are in good agreement with theoretical predictions for wormlike cylinders. The first order in volume fraction (ϕ) coefficient K of the ϕ-dependent sedimentation coefficient $s(\phi) = 1 - K\phi$ decreases from 1178 for the shortest fragment to 882 for the longest fragment. These values are much larger than predicted for uncharged rigid rods, indicating the presence of associates with an enhanced aspect ratio and excluded volume. The precise match of the molecular weights obtained from exponential sedimentation–diffusion equilibrium distributions with weights calculated from the number of base pairs shows that any association is reversible and disappears at sufficiently low DNA concentration.

Keywords: Analytical ultracentrifugation; Monodisperse DNA; Sedimentation velocity/equilibrium; Rigid/semiflexible rods

1. Introduction

Due to the well-defined structure of DNA and the possibility to produce homologous series of monodisperse molecules using molecular cloning techniques [1], double-stranded (ds) DNA is widely used as a model for a wormlike polyelectrolyte. Several studies have addressed static properties of DNA solutions, including the molecular conformation and intermolecular interactions [2–5] and mesophase formation [6–8]. Transport properties investigated include mutual diffusion [3–5,9–11], self-diffusion [12], rotational diffusion [13–15], rheology [5,16], and sedimentation [9,17]. A systematic study of the length and concentration dependence of the transport properties of DNA molecules and a comparison with theoretical models for semiflexible polymers is, however, still lacking.

Our aim is to elucidate the length and concentration dependence of the sedimentation velocity of semiflexible polymers using a model system of monodisperse, blunt-ended, linear, ds-DNA restriction fragments. In Part I of this work we describe the design, preparation, and purification of a homologous series of DNA fragments with contour lengths L_c that span a range of flexibilities L_c/q from 3 to 11. Here we report sedimentation velocity measurements, which are compared with hydrodynamic theories for the transport properties of uncharged semiflexible [18,19] and rigid rodlike [20–22] polymers. The infinite dilution sedimentation

* Corresponding author. Fax: +31 30 2533870.
E-mail address: fccoffice@chem.uu.nl (A.P. Philipse).
[1] Present address: CBR Institute, Harvard University, 800 Huntington Ave., Boston, MA 02115, USA.

0021-9797/$ – see front matter
doi:10.1016/j.jcis.2005.04.114

coefficients are compared with earlier results obtained by Kovacic and Van Holde [17] on restriction fragments with 50 to 1735 bp. Studies of the concentration dependence of sedimentation were thus far restricted to 150 bp mononucleosomal DNA [9]. We furthermore performed sedimentation–diffusion equilibrium measurements, to determine the molecular weights of the fragments independently and to verify the purity of the DNA preparations. We study aqueous saline solutions of DNA containing 100 mM Na^+, so the electrostatic contribution to the persistence length q is negligible and the total persistence length q is ca. 50 nm [11,23].

2. Theoretical background

2.1. Sedimentation of non-interacting semiflexible polymers

Experimentally determined sedimentation velocities U_0 for dilute solutions are usually converted to sedimentation coefficients, s_0, which can be expressed as

$$s_0 \equiv \frac{U_0}{\Omega^2 r} = \frac{\mathrm{d}r/\mathrm{d}t}{\Omega^2 r} = \frac{M(1-V_\mathrm{p}\rho_\mathrm{s})}{N_\mathrm{av} f_0^\mathrm{t}}, \tag{1}$$

with Ω the angular velocity, r the distance from the center of rotation, M the molar mass, V_p the partial specific volume, and ρ_s the mass density of the solvent. Equation (1) results from the balance between the centrifugal or gravitational force acting on the effective buoyant mass $M(1-V_\mathrm{p}\rho_\mathrm{s})/N_\mathrm{av}$, and the frictional force $F_\mathrm{drag} = -f_0^\mathrm{t} U_0 = -f_0^\mathrm{t}\,\mathrm{d}r/\mathrm{d}t$. In the latter expression f_0^t represents the Stokes friction factor. Derivations of Eq. (1) can be found in textbooks and additional information may be found in [24]. We would like to point out that in Eq. (1) the partial specific volume has to be used, which is the increase in volume of the solution upon adding solute, $(\delta V/\delta g)_{\mathrm{T,P,g1}}$. Subscripts T, P, and g1 specify that the temperature, pressure, and mass of solvent are held constant. The partial specific volume is not the volume of the hydrated solute, which is used to model the friction factor, divided by its mass. For an impermeable object the increase in the volume of the solution is just equal to the volume of added solute, and therefore the partial specific volume is equal to the specific volume (inverse of the mass density). For DNA the density depends on the pH and salt concentration. We use in Eq. (1) 0.556 $\mathrm{cm^3\,g^{-1}}$ for the partial specific volume of DNA in 100 mM aqueous saline solution [3,4,9,18,25].

In a sedimentation velocity experiment the displacement of the boundary r_b in time is measured. Rearrangement of Eq. (1) gives

$$\frac{\mathrm{d}r_\mathrm{b}}{\mathrm{d}t} = s\Omega^2 r, \tag{2}$$

which when integrated yields

$$\ln\bigl[r_\mathrm{b}(t)/r_\mathrm{b}(t_0)\bigr] = s\Omega^2(t-t_0), \tag{3}$$

with $r_\mathrm{b}(t_0)$ the position of the meniscus. The sedimentation coefficient is obtained from a plot of $\ln(r_\mathrm{b})$ versus $\Omega^2 t$, which should give a straight line with slope s.

To facilitate comparison with literature values, the sedimentation coefficients s_0 are usually converted to standard values s_w^{20} for water as a solvent using

$$s_{0\mathrm{w}}^{20} = s_{0\mathrm{b}}\frac{(1-V_\mathrm{p}\rho_\mathrm{w})}{(1-V_\mathrm{p}\rho_\mathrm{s})}\frac{\eta_0}{\eta_\mathrm{w}}. \tag{4}$$

The Stokes friction factor f_0^t is a function of the size and shape of the particles. For a sphere of diameter d_T in a solvent of viscosity η_0, f_0^t is $3\pi\eta_0 d_\mathrm{T}$. Stiff rodlike particles experience a considerably larger Stokes drag. Earlier sedimentation [9,17] as well as translational diffusion [10,11] measurements on monodisperse DNA fragments of up to 2311 bp have shown that the Stokes drag is predicted correctly by the Yamakawa–Fujii [18] theory for smooth wormlike cylinders without excluded volume and neglecting end-effects. The orientationally averaged friction coefficient of a wormlike Brownian cylinder of contour length L_c, diameter D, and persistence length q resembles the friction factor for a sphere but contains an additional term, $F(D, L_\mathrm{c}, q)$, that is affected by the actual shape [18]:

$$f_0^\mathrm{t} = 3\pi\eta_0 L_\mathrm{c}\bigl[F(D, L_\mathrm{c}, q)\bigr]^{-1}. \tag{5}$$

Expressions and numerical results for $F(D, L_\mathrm{c}, q)$ can be found in Appendix A, Eqs. (A.1) and (A.2). Numerical results were obtained using a hydrated diameter [17] of 2.6 nm, a rise per base pair [26] of 0.337 nm and a molecular mass per unit length [27] $M_\mathrm{L} = 1950\ \mathrm{Da\,nm^{-1}}$. The friction factor of a wormlike chain decreases continuously with increasing chain length from the drag of a rigid rod, q being infinite (Appendix B, Eq. (B.1)), to the drag of a long infinitely flexible chain, q being almost zero (Appendix B, Eq. (B.2)). The rigid rod limit of Eq. (5) (see Eq. (B.1) in Appendix B) is in good agreement with numerical results of Tirado et al. [20] (Appendix B, Eq. (B.3)) for rigid rods with aspect ratio L_c/D between 2 and 30. Furthermore, the Yamakawa–Fujii theory ignores end-effects, which are indeed negligible for chains with aspect ratios down to 4 [19].

The predicted Stokes drag of DNA fragments is fairly insensitive to small bending fluctuations, being equal to the rigid rod friction factor up to $L_\mathrm{c}/q \cong 1$ (200 bp), as shown in Fig. 4. Indeed, the sedimentation velocity [9,17] as well as the translational diffusion coefficient [3,5,9,12] of DNA fragments of up to 200 bp have been shown to still obey rigid-rod behavior. However, DNA fragments of one persistence length cannot actually be considered as rigid rods [23]. This point may be illustrated by considering the mean-square end-to-end distance of a wormlike chain described by the Kratky–Porod expression [28]

$$\langle R^2\rangle = 2q^2\left\{\frac{L_\mathrm{c}}{q} - 1 + \exp(-L_\mathrm{c}/q)\right\}. \tag{6}$$

In case $L_\mathrm{c} = q$, the root-mean-square end-to-end distance is only 86% of the contour length. The rotational Stokes fric-

tion factor is significantly more sensitive to flexibility effects than the translational drag. The rotational diffusion time begins to depart from rigid-rod behavior already for fragments of more than 120 bp, as shown by transient electric birefringence [14] and triplet anisotropy decay [29] measurements.

2.2. Sedimentation of interacting semiflexible polymers

At finite concentration, hydrodynamic and direct interactions between the particles affect their sedimentation velocity. At low volume fractions ϕ, the sedimentation coefficient of uncharged particles is usually linear in ϕ:

$$s/s_0 = 1 - K\phi. \tag{7}$$

The magnitude of K is mainly determined by solvent backflow arising from the walls of the container in which the particles settle. There is extensive literature concerned with the concentration dependence of the sedimentation of spherical colloidal particles [30]. For monodisperse hard spheres, Batchelor [31] showed that $K = 6.55$. K is very sensitive to deviations of the interaction potential $U(r)$ from a hard-particle potential. Weak attractions reduce K, due to mutual screening of the particles from solvent backflow. Long-range repulsive forces lead to values of K larger than 6.55, because the well-separated particles are fully exposed to the retarding solvent backflow produced by the sedimenting particles.

We are not aware of any calculations of K for wormlike cylinders, so we compare our data with theories [21,22] for rigid rods.

Hydrodynamic interactions (HI) must be computed for pairs of rods at arbitrary orientation, therefore the concentration dependence of rod sedimentation is difficult to calculate exactly and accurate expressions for the HI tensors for rigid or semiflexible rods are still lacking. Peterson [21] performed the first approximate calculation of the leading-order concentration dependence of the sedimentation velocity of rigid rods, based on approximate pre-averaged pair HI, and modeling the rods as linear arrays of touching spherical beads:

$$K = \frac{8(3/8)^{2/3}(L_c/D)^{1/3}}{2\ln(L_c/D)}\frac{L_c}{D}, \quad L_c/D \gg 1. \tag{8}$$

Due to the relatively large excluded volume of a rod, the concentration dependence of the sedimentation velocity is more pronounced for long rods than for spheres. Recently, Dhont [22] presented more accurate calculations of the leading-order concentration dependence, without pre-averaging the HI and taking more accurate account of solvent backflow. Employing HI tensors for rigid rods, treated as strings of spherical beads, within a mean-field approximation valid for dilute suspensions of long and thin rods, Dhont's result for K reads

$$K = \frac{6.4 + 2/9(L_c/D)}{2\ln(L_c/D) - (\nu_\perp + \nu_\parallel)}\frac{L_c}{D}, \quad L_c/D \gg 1, \tag{9}$$

with constants $\nu_\perp = -0.84$ and $\nu_\parallel = 0.21$ for cylindrical rods. For aspect ratios higher than 30, Eq. (9) predicts a much larger K than Eq. (8). Equation (9) was found to be in fair agreement with experimental values for filamentous bacteriophage *fd* virus ($L_c/D = 130$) and rigid silica rods ($L_c/D = 13$ and 24) [22].

2.3. Sedimentation equilibrium measurements

Sedimentation–diffusion equilibrium measurements on a dispersion or solution of particles yield the equilibrium concentration distribution of particles that is formed when transport by sedimentation in a gravitational or centrifugal field is balanced by diffusional transport due to the osmotic pressure. The equilibrium distribution is independent of frictional properties and reflects thermodynamic particle interactions. For dilute dispersions of ideal particles in a centrifugal field this distribution can be described by the single exponential Boltzmann function,

$$A(r) = A(r_0)\exp\left[M\Omega^2(1 - V_p\rho_s)\left(r^2 - r_0^2\right)/2RT\right], \tag{10}$$

with $A(r)$ the particle concentration (measured, for instance, as optical absorbance) at a radial distance r from the axis of rotation, where r_0 refers to a position near the meniscus. Measurements of $A(r)$ yield the molar weight M of the particles.

3. Materials and methods

3.1. Colloidal model system

We studied a homologous series of monodisperse, blunt-ended ds-DNA restriction fragments of 400, 800, and 1600 base pairs (bp), dissolved in TEN_3 buffer of pH 7.5 containing 10 mM Tris-HCl, 1 mM EDTA, 99 mM NaCl, and 7.6 mM NaN_3. A detailed description of the synthesis, purification, and characterization of the DNA fragments is presented in Part I.

3.2. Sedimentation measurements

Sedimentation experiments were performed with a Beckman Optima XL-A analytical ultracentrifuge using standard 12 mm double-sector centerpiece cells in an An-50 Ti rotor, at a constant temperature of $20 \pm 0.1\,^\circ$C. The concentration profiles of the sedimenting fragments across the cells were monitored using the characteristic absorption of DNA around 260 nm. The exact wavelength was chosen depending on the DNA concentration, which was determined from the optical density (OD) at 260 nm, to give an initial OD of 0.5–1.2 for sedimentation velocity and 0.1–0.5 for sedimentation equilibrium measurements.

Sedimentation equilibrium profiles were obtained at $20 \pm 0.1\,^\circ$C by prolonged centrifugation of samples containing 22 to 24 $\mu g\,ml^{-1}$ DNA at 3000, 4500, and 6000 rpm. Concentration profiles at each angular velocity were recorded at three different wavelengths ranging from 265 to 281 nm.

Equilibrium was supposed to be reached when a straight line was obtained by subtracting a profile from another profile recorded 8 h before. Equilibrium was usually reached after more than one week of centrifugation. Using Microcal Origin 3.85 the Boltzmann equation (Eq. (10)) for an ideal one-component system was fitted to the recorded equilibrium profiles,

$$\mathrm{OD}\left(r^2 - r_{\mathrm{meniscus}}^2\right) = \exp\left[\ln(A) + CM\left(r^2 - r_{\mathrm{meniscus}}^2\right)\right] + \mathrm{Baseline}, \quad (11)$$

with OD the optical density (extinction), Baseline the OD value of the flat part of the profile, and A and C constants depending on Ω^2, the gas constant R, the partial specific volume of the solute, and the mass density of the buffer.

For sedimentation velocity measurements, the samples containing 24 to 520 µg ml^{-1} DNA were centrifuged at 35,000–40,000 rpm for 3–5 h, depending on the fragment's molecular weight. Sedimentation coefficients were determined from the displacement velocity $\mathrm{d}r_{\mathrm{b}}/\mathrm{d}t$ (Eq. (3)) of the sedimentation boundary observed in 35 scans taken at different points in time. Sedimentation boundary positions r_{b} were obtained by the second moment method [32] using the Beckman XL-A software version p4.5. Sedimentation coefficients at infinite dilution, $s_{0,\mathrm{b}}$, were determined by extrapolating the sedimentation data to zero concentration. All coefficients were converted to standard values s_{w}^{20} for water (Eq. (4)), using the mass density $\rho_{\mathrm{w}} = 0.99821$ g ml^{-1} and viscosity $\eta_{\mathrm{w}} = 1.002$ mPa s of water [33] and the measured mass density $\rho_{\mathrm{s}} = 1.00334$ g ml^{-1} (Anton-Paar densitometer) and viscosity $\eta_{\mathrm{w}} = 1.020$ mPa s (Ubbelohde capillary viscometer) of the buffer.

4. Results and discussion

4.1. Sedimentation equilibrium experiments

Typical equilibrium concentration profiles of the three DNA fragments consisting of 400, 800, and 1600 base pairs are shown in Fig. 1. Note that the profiles were not recorded at the same angular velocity and that the absorbance was measured at different wavelengths. A plot of the natural logarithm of the absorbance versus the radial position squared should give a straight line characteristic of a single exponential function. The equilibrium profiles of all fragments have two straight regions, one in the bottom of the cell due to the DNA restriction fragments, and one in the top due to low molecular weight contaminants of approximately 3–5 kDa, corresponding to small DNA fragments of 4 to 5 bp (assuming ds-DNA) (Fig. 2). Additional evidence for the presence of low molecular weight contaminants, most likely deoxynucleoside monophosphates (dNMPs) originating from partial degradation of the DNA fragments, is presented in Part I of this work.

The molar weights obtained from the fits (gray lines in Fig. 1) are shown in Table 2 together with the theoretically

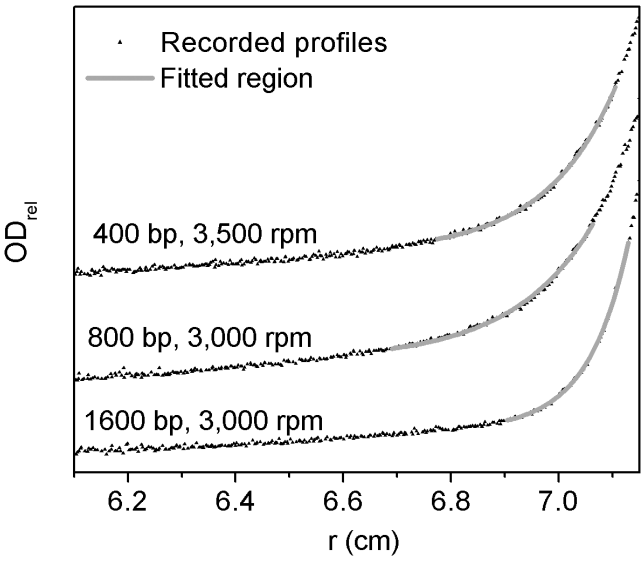

Fig. 1. Three typical equilibrium optical absorbance profiles for DNA fragments with 400, 800, and 1600 base pairs. The gray lines are nonlinear least-square fits using Eq. (11).

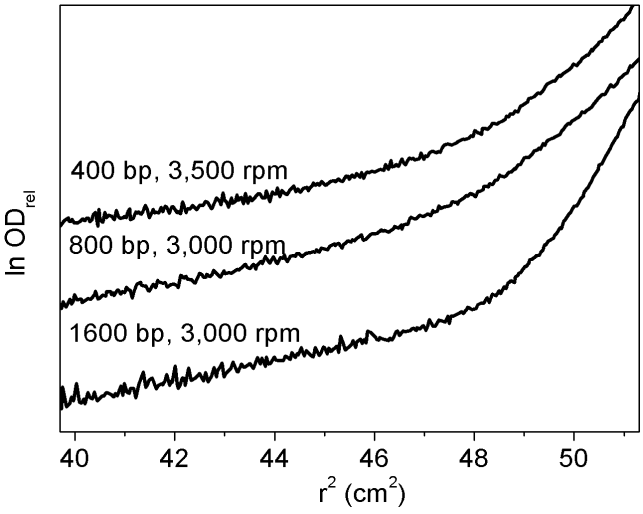

Fig. 2. A plot of the natural logarithm of the absorbance versus the radial position squared. In the upper part of the profiles, i.e., the range from 40 to 47 cm^2, low molecular weight contaminants are evident.

calculated values (see also Table 1). The experimentally determined molar weights of all three fragments are close to their theoretical values. This shows that the DNA fragments at low concentration (below 25 µg ml^{-1}) do not form any associates (aggregates), in contrast to more concentrated DNA solutions.

4.2. Sedimentation velocity experiments

Fig. 3 shows representative sequences of sedimentation profiles measured for dilute (A) and concentrated (B) solutions of 400 bp DNA fragments in buffer. The sedimentation boundaries broaden appreciably with time as they progress toward the bottom of the cell. If the sedimenting units are

Table 1
Characteristics of the DNA restriction fragments

N_{bp}[a]	L_c [nm][b]	L_c/q[c]	p[d]	M [kg mol^{-1}][e]	R_g [nm][f]	c^* [mg ml^{-1}][g]	c_i [mg ml^{-1}][h]
400	135	2.70	52	262.9	31	3.4	116
800	270	5.40	104	525.7	52	1.4	58
1600	539	10.80	207	1051.4	83	0.7	29

[a] Number of base pairs (bp).
[b] Contour length, calculated as $L_c = N_{bp} r_{bp}$, where $r_{bp} = 0.337$ nm is the rise per base pair for the Na^+ form of B-DNA [26].
[c] Number of persistence lengths per chain, $N_k = L_c/q$, where $q = 50$ nm is the persistence length of ds-DNA in a buffer containing 100 mM Na^+ [23].
[d] Rigid-rod aspect ratio $p = L_c/D$, where D is the hydrated diameter of 2.6 nm [17].
[e] Molar weight, calculated from the contour length by multiplication with the linear molecular weight density $M_L = 1950$ Da nm^{-1} [18].
[f] Radius of gyration calculated from the Benoit–Doty formula [34] for a Kratky–Porod [28] wormlike chain. Excluded volume interactions are negligible for duplex DNA of less than around 10 kbp [35].
[g] Overlap concentration, calculated according to $c^* = 3M/(N_{av} 4\pi R_g^3)$.
[h] Concentration where nematic phase starts to form according to the Onsager theory [36] for long rigid hard rods ($c_i = 4.25(\pi/4)(D/L_c) \times 10^3/0.556$).

Table 2
Comparison of theoretical molar weights and molar weights obtained from sedimentation velocity and equilibrium measurements

Fragment	Sedimentation velocity [18]		Sedimentation equilibrium			Theory	
	M (kg mol^{-1})	N_{bp}	M (kg mol^{-1})	N_{bp}	Profiles #	M (kg mol^{-1})	N_{bp}
400 bp	333.2	507	257.7 ± 9.7	392	9	262.9	400
800 bp	575.7	876	509.4 ± 27.5	775	9	525.7	800
1600 bp	1081.0	1645	1043.9 ± 4.9	1588	6	1051.4	1600

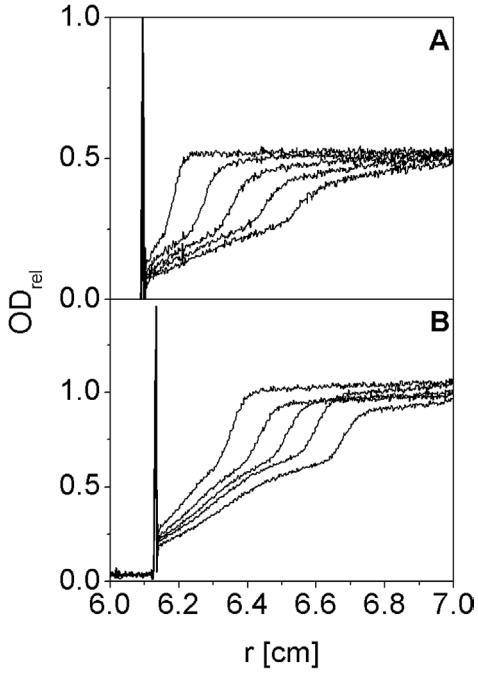

Fig. 3. Typical time series of absorbance profiles of sedimenting DNA solutions in buffer as a function of radial position, obtained during centrifugation at a speed of 40,000 rpm. The absorbance (OD_{rel}) is measured relative to the buffer absorbance. The direction of sedimentation is from left to right. (A) Dilute, 25 μg ml^{-1}; (B) concentrated, 441 μg ml^{-1}; solution of 400 bp DNA.

unaggregated monodisperse DNA fragments, this broadening is entirely due to diffusion of the sedimenting particles, which opposes the formation of a concentration gradient by the centrifugal field.

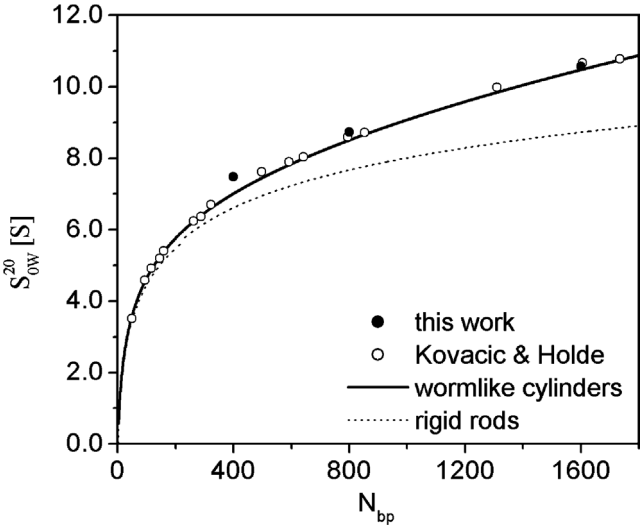

Fig. 4. Infinite dilution sedimentation coefficients s^{20}_{0w} of non-interacting ds-DNA fragments measured in this (closed circles) and previous [17] (open circles) work, compared with the theoretical predictions for smooth wormlike cylinders [18] and rigid rods [20].

With increasing molar mass, the sedimentation coefficient s^{20}_{0w} increases, see Fig. 4. The data are in good agreement with data obtained by Kovacic and Van Holde [17] on a series of ds-DNA restriction fragments with 50 to 1735 base pairs prepared by digestion of phage DNA and dissolved in a buffer containing 195 mM Na^+. The theoretical predictions for wormlike [18] and rigid-rod [20] cylinders, respectively, diverge for fragments longer than 200 bp. The experimental data asymptotically approach the theoretical prediction for uncharged rigid rods (solid line) at low molar mass and are

Table 3
Experimental and theoretical sedimentation coefficients s^{20}_{0w} of DNA restriction fragments in water at 20 °C and at infinite dilution (in Svedberg units of 10^{-13} s) and first-order concentration coefficients K

N_{bp}	Experimental		Rigid rod		Wormlike cylinder
	s^{20}_{0w}	K	s^{20}_{0w} (Tirado)	K (Dogic)	s^{20}_{0w} (Yamakawa–Fujii)
400	7.48 ± 0.04	1178 ± 58	6.54	118	7.02
800	8.73 ± 0.08	1008 ± 49	7.59	329	8.52
1600	10.57 ± 0.02	882 ± 21	8.65	1020	10.47

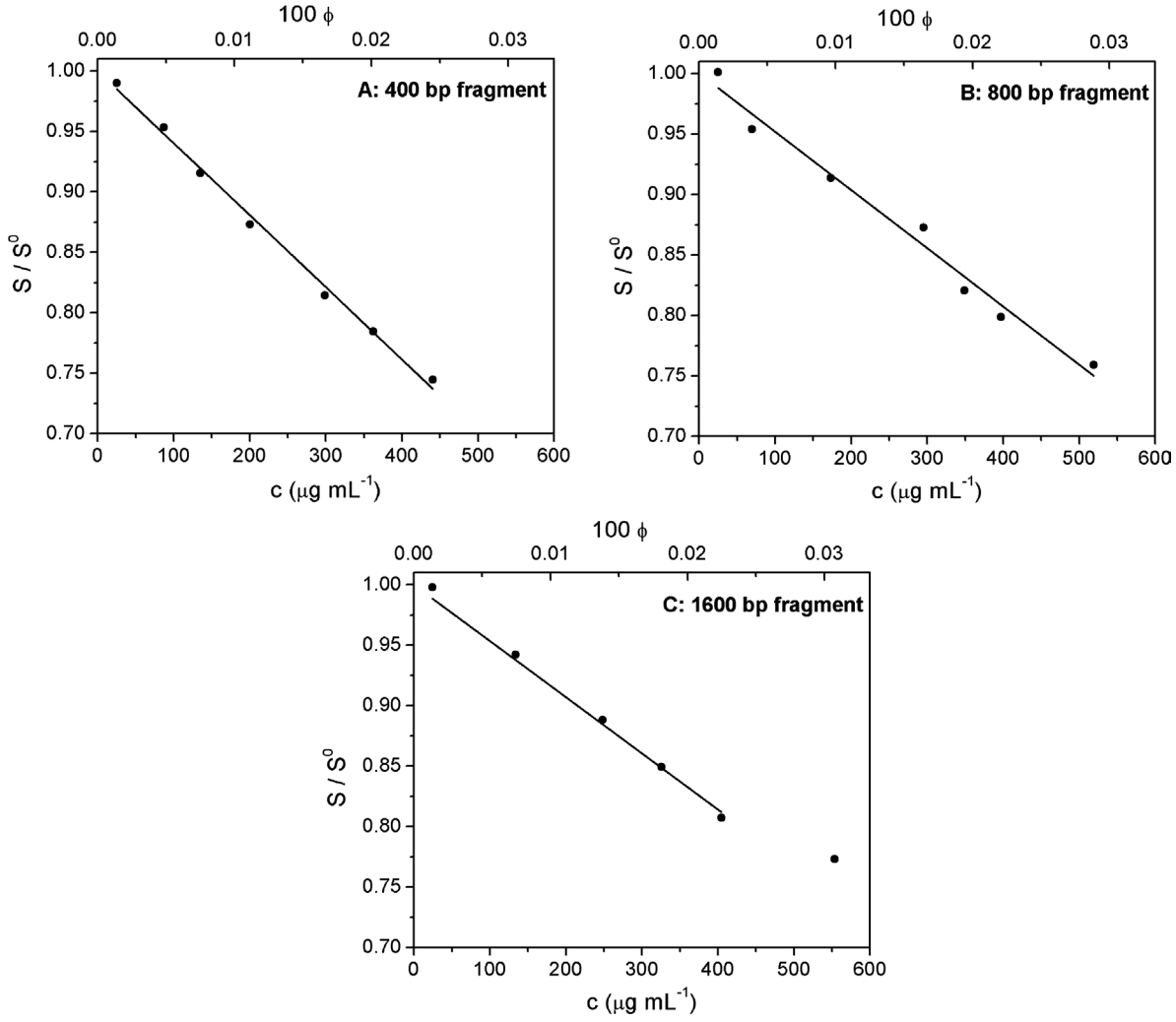

Fig. 5. Concentration dependence of the reduced sedimentation coefficient s/s_0 for fragments of (A) 400, (B) 800, and (C) 1600 base pairs. Solid lines are linear least-square fits.

in overall good agreement with the Yamakawa–Fujii theory for wormlike cylinders (see also Table 3).

It should be noted that the sedimentation velocity measurements overestimate the molar weight, while sedimentation equilibrium measurements give molar weights that are closer to and somewhat lower than the expected values (Table 2). The sedimentation equilibrium measurements are more sensitive to low molecular weight contaminants than sedimentation velocity measurements. The position of the sedimenting boundary in the sedimentation velocity measurements is unaffected by the presence of low molecular weight contaminants, which show up in the lower plateaus in Fig. 3. In contrast, the equilibrium concentration profiles are clearly multi-exponential functions (Fig. 2).

The concentration dependence of the sedimentation coefficients was studied for DNA concentrations up to 550 μg ml^{-1}, which is far below the critical concentrations for overlap (c^*) and for an isotropic-nematic phase transition (see Table 1), and also below the onset of visible aggregation. Fig. 5 shows that over the concentration range studied

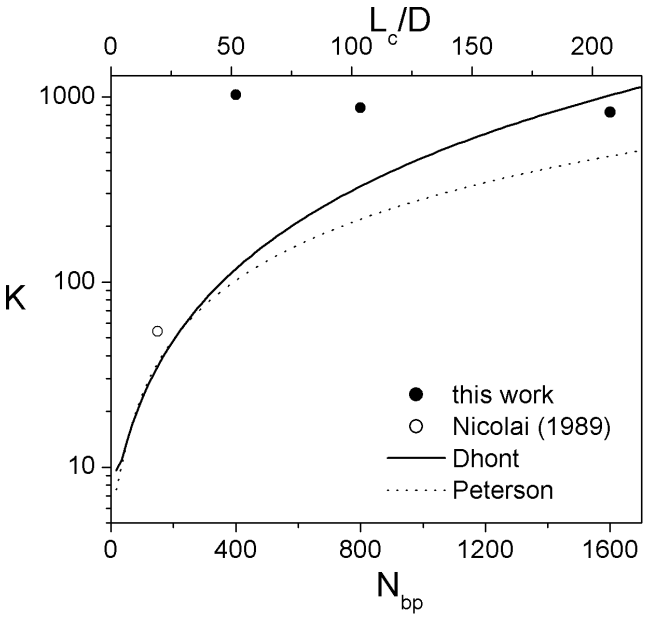

Fig. 6. Leading order in volume fraction coefficient K of $s(\phi)$ as a function of the fragment length (in terms of the number of base pairs, N_{bp}, or the aspect ratio, L_{c}/D). Solid and dotted lines represent theoretical results for uncharged rigid rods by Dhont [22] and Peterson [21]. The open circle represents a measurement of Nicolai and Mandel [9] on a 150 bp mononucleosomal DNA fragment in buffer containing 0.5 M NaCl at 25 °C.

the sedimentation coefficient is within experimental error linear in the DNA concentration. The leading order in volume fraction ($\phi = cV_{\mathrm{p}}$) coefficient K decreases from 1178 for 400 bp to 882 for 1600 bp, as shown in Fig. 6 (see Table 3).

The predictions by Dhont [22] and Peterson [21] are expected to overestimate the concentration coefficient of wormlike cylinders. Yet, the experimental values for the 400 and 800 bp fragments are considerably above the rigid-rod prediction. The 400 bp fragment is the least flexible, but nevertheless exhibits the largest (relative and absolute) deviation from Dhont's prediction for rigid rods. Such a large K value suggests an excluded volume of sedimenting species that is much larger than that of an individual 400 bp fragment. Residual double-layer repulsions between the negatively charged DNA filaments may contribute to this excluded volume. Static light scattering measurements of the second virial coefficient B_2 of short (150 bp) DNA fragments in aqueous NaCl solutions [2,3,5] show that B_2 still decreases on going from 100 to 500 mM NaCl. Interpretation of these measurements in the light of theory for charged rigid rods suggests that the effective diameter of ds-DNA in the presence of 100 mM NaCl is about 5 nm, which is significantly larger than its hydrodynamic diameter of 2.6 nm. Long-range repulsions enhance K by keeping the particles well separated, exposing them to solvent backflow. However, this effect is insufficient to match the discrepancy seen in Fig. 6. The value of $K = 1178$ corresponds, according to Dhont's equation (9), to a thin rod with an effective aspect ratio four times that of the 400 bp fragment. This rather suggests the presence of linear associates of fragments.

It is interesting to note that such linear association would significantly increase K but hardly affect s_0. Since the mass M of linear associates is proportional to the length L_{c}, s_0 in Eq. (1) scales as $s_0 \propto \ln(L/D)$ for rigid thin rods, and as $s_0 \propto L^{1/2}$ for long flexible chains. In particular, s_0 of thin rods is rather insensitive to linear association, mainly because the increase in mass is balanced by the increase in friction. The effect on K, however, is much more pronounced. Suppose rods with aspect ratio p form linear α-mers with aspect ratio αp. Let K_p and $K_{\alpha p}$ denote the values from Dhont's equation (9) for the 400 bp fragment and the α-mer, respectively. For $p \gg 1$ we find

$$K_{\alpha p} \cong \frac{\alpha^2}{\ln \alpha} K_p, \tag{12}$$

which would imply $K_{\alpha p} \cong 11.5 K_p$ for a fourfold aspect ratio increase. For the 400 bp fragment in Fig. 6 this corresponds to $K_p \cong 102$, close to Dhont's prediction. For the longer fragments in Fig. 6 such a correction based on an effective rigid rod on Dhont's curve works less well, most likely because of the increasing degree of flexibility of the DNA fragments with increasing length. This argument does not conclusively prove that 400 bp fragments are associated into entities with an equivalent rigid-rod aspect ratio of $4p$. It merely shows that linear association could account for a drastic increase of K. Further measurements, particularly dynamic light scattering and fluorescence recovery after photobleaching, are needed to assess any association.

The measurement of Nicolai and Mandel [9] on a 150 bp mononucleosomal DNA fragment in buffer containing 0.5 M NaCl at 25 °C deviates less from the rigid-rod prediction ($K = 35$) compared to our data. The value of $K = 54$ obtained by Nicolai was found by linear curve fitting of three data points obtained at DNA concentrations of 0.004, 6.5, and 10.5 mg ml^{-1}. If we assume that the fragment behaves like an uncharged rigid rod, the model of linear associates combined with the Dhont theory suggests sedimentation units in samples with a DNA concentration above 25 μg ml^{-1} with an equivalent rigid-rod aspect ratio of 1.5.

5. Summary and conclusions

We report ultracentrifugation measurements of the sedimentation velocity and sedimentation–diffusion equilibrium of monodisperse, double-stranded, and blunt-ended DNA restriction fragments of 3 to 11 persistence lengths in aqueous buffer containing 99 mM NaCl (107 mM Na^+). The molar weights of the fragments determined from sedimentation equilibrium and velocity measurements agree well with the expected values, though the equilibrium measurements demonstrate the presence of low molecular weight

contaminants, possibly originating from partial DNA degradation. The infinite dilution sedimentation coefficients s_0 agree well with theoretical predictions for non-interacting wormlike cylinders. The first order in volume fraction coefficients K of the concentration-dependent sedimentation coefficients $s(\phi)$ are much larger than predicted for uncharged rigid rods, indicating that the sedimenting species have a much larger excluded volume than individual fragments. Residual double-layer repulsions may contribute to this excluded volume but cannot explain the very large K values, which are very likely due to linear associates with an effectively larger aspect ratio, an increase that hardly affects s_0. Within a simple model of linear, rigid-rod associates, s_0 is rather insensitive to association while K increases strongly with an increasing degree of association. Comparison with the theory for rigid rods suggests for the 400 bp fragment linear associates with an aspect ratio four times that of the fragment. For the longer fragments bending fluctuations become more important. The sedimentation equilibrium measurements as well as the sedimentation velocities at infinite dilution unequivocally demonstrate that at low concentrations around 25 $\mu g\,ml^{-1}$ no aggregates or associates are formed. Thus, the association behavior of the DNA restriction fragments is concentration dependent.

Further measurements, particularly dynamic light scattering and t-FRAP, could be used to determine the translational diffusion coefficient independently from sedimentation measurements. Finally, it would be interesting to compare the reported measurements on blunt-ended fragments with corresponding measurements for sticky-end fragments, for which the interactions may be tuned by varying the temperature.

Acknowledgments

Dr. D. Thies-Weesie, Dr. I. Validzic-Mladenovic, and Dr. L. Rutten are acknowledged for their help with the AUC measurements, Dr. D. van der Beek for help with Ubbelohde measurements, and Dr. D. Thies-Weesie for assistance with density measurements. This work was financially supported by The Netherlands Organization for Scientific Research (NWO/Stichting Chemische Wetenschappen).

Appendix A

The expression for $F(D, L_c, q)$ of a wormlike cylinder for contour lengths $L_c > 4.556q$ has the form [18]

$$F = A_1\left(\frac{L_c}{2q}\right)^{1/2} + A_2 + A_3\left(\frac{L_c}{2q}\right)^{-1/2} + A_4\left(\frac{L_c}{2q}\right)^{-1} + A_5\left(\frac{L_c}{2q}\right)^{-3/2}, \tag{A.1}$$

while for contour lengths $L_c \leqslant 4.556q$ [18]

$$\begin{aligned} F = {} & C_1 \ln\left(\frac{L_c}{D}\right) + C_2 + C_3\left(\frac{L_c}{2q}\right) + C_4\left(\frac{L_c}{2q}\right)^2 \\ & + C_5\left(\frac{L_c}{2q}\right)^3 + C_6\frac{D}{L_c}\ln\left(\frac{L_c}{D}\right) + C_7\left(\frac{D}{L_c}\right) \\ & + C_8\left(\frac{D}{L_c}\right)^2 + C_9\left(\frac{D}{L_c}\right)^3 + C_{10}\left(\frac{D}{L_c}\right)^4 \\ & + O\left[\left(\frac{D}{L_c}\right)^5\right]. \end{aligned} \tag{A.2}$$

Note that the original paper of Yamakawa and Fujii [18] contains a misprint in their Eq. (49) (here Eq. (A.1)) having a term $A_1 L_c^{-1/2}$ instead of $A_1 L_c^{1/2}$, and the closing bracket of the argument of the logarithm in the C_6 term in their Eq. (51) (here Eq. (A.2)) is omitted. The explicit numerical results of Yamakawa and Fujii [18] for the coefficients appearing in Eqs. (A.1) and (A.2) for the translational friction coefficient of wormlike cylinders are summarized below. Additionally, numerical results for DNA are provided. The coefficients for short cylinders ($L \leqslant 4.556q$), in terms of $d \equiv D/(2q)$, are

$$\begin{aligned} C_1 &= 1 - 0.01412d^2 + 0.00592d^4 + O(d^6) = 0.99999, \\ C_2 &= 0.3863 - 0.1667d + 0.0016d^2 - 0.0224d^3 \\ &\quad - 0.0007d^4 + O(d^5) = 0.38197, \\ C_3 &= 0.1667 + 0.0222d^2 + 0.0017d^4 + O(d^6) = 0.16672, \\ C_4 &= 0.01883 - 0.00789d^2 - 0.00038d^4 + O(d^6) \\ &= 0.01882, \\ C_5 &= -0.002039 + 0.000805d^2 + 0.000017d^4 + O(d^6) \\ &= -0.00204, \\ C_6 &= 0.04167d + 0.00567d^3 + 0.00592d^4 + O(d^5) \\ &= 0.00108, \\ C_7 &= 0.5 + 0.0786d - 0.0094d^2 + 0.0107d^3 + 0.0039d^4 \\ &\quad + O(d^5) = 0.50204, \\ C_8 &= -0.06250 + 0.00132d^2 - 0.00055d^4 + O(d^6) \\ &= -0.0625, \\ C_9 &= 0.001302d + 0.000181d^3 + O(d^5) = 3.3855 \times 10^{-5}, \\ C_{10} &= 0.001953 - 0.000064d^2 + 0.000027d^4 + O(d^6) \\ &= 0.00195. \end{aligned}$$

The coefficients for longer chains ($L > 4.556q$) read

$$\begin{aligned} A_1 &= \frac{4}{3}\left(\frac{6}{\pi}\right)^{1/2} = 1.84264, \\ A_2 &= -\left[1 - 0.01412d^2 + 0.00592d^4 + O(d^6)\right]\ln(d) \\ &\quad - 1.0561 - 0.1667d - 0.1900d^2 - 0.0224d^3 \\ &\quad + 0.0190d^4 + O(d^5) = 2.58906, \\ A_3 &= 0.1382 + 0.6910d^2 = 0.13867, \\ A_4 &= -\left[0.04167d^2 + 0.00567d^4 + O(d^6)\right]\ln(d) \end{aligned}$$

$$-1.0561-0.3301+0.5d-0.5854d^2-0.0094d^3$$
$$-0.0421d^4+O(d^5)=-0.31739,$$
$$A_5=-0.0300+0.1209d^2+0.0259d^4=-0.02992.$$

Appendix B

Equations (A.1) and (A.2) illustrate that the friction factor of a wormlike chain decreases continuously, with increasing chain length, from the drag of a rigid rod (q is infinite),

$$F\approx C_1\ln\left(\frac{L_c}{D}\right)+C_2=\ln\frac{L_c}{D}+0.3863, \tag{B.1}$$

to the drag of a long infinitely flexible chain (q is almost zero),

$$F\approx A_1\left(\frac{L_c}{2q}\right)^{1/2}+A_2=\frac{4}{3}\left(\frac{6}{\pi}\right)^{1/2}\left(\frac{L_c}{2q}\right)^{1/2}. \tag{B.2}$$

The rigid-rod limiting expression, Eq. (B.1), is in good agreement with numerical results of Tirado et al. [20] for rigid rods with aspect ratio L_c/D between 2 and 30:

$$F=\ln\frac{L_c}{D}+0.312+0.565\frac{D}{L_c}-0.100\left(\frac{D}{L_c}\right)^2. \tag{B.3}$$

The Yamakawa–Fujii theory ignores end-effects, which are indeed negligible for chains with aspect ratios down to $L_c/D=4$ [19].

References

[1] R.J. Lewis, J.H. Huang, R. Pecora, Macromolecules 18 (1985) 1530.
[2] T. Nicolai, M. Mandel, Macromolecules 22 (1989) 438.
[3] H.T. Goinga, R. Pecora, Macromolecules 24 (1991) 6128.
[4] M.E. Ferrari, V.A. Bloomfield, Macromolecules 25 (1992) 5266.
[5] P. Wissenburg, T. Odijk, P. Cirkel, M. Mandel, Macromolecules 28 (1995) 2315.
[6] K. Kassapidou, W. Jesse, J.A.P.P. Van Dijk, J.R.C. Van der Maarel, Biopolymers 46 (1998) 31.
[7] R. Podgornik, H.H. Strey, K. Gawrisch, D.C. Rau, A. Rupprecht, V.A. Parsegian, Proc. Natl. Acad. Sci. USA 93 (1996) 4261.
[8] K. Merchant, R.L. Rill, Biophys. J. 73 (1997) 3154.
[9] T. Nicolai, M. Mandel, Macromolecules 22 (1989) 2348.
[10] S.S. Sorlie, R. Pecora, Macromolecules 23 (1990) 487.
[11] H. Liu, J. Gapinski, L. Skibinska, A. Patkowski, R. Pecora, J. Chem. Phys. 113 (2000) 6001.
[12] L. Wang, M.M. Garner, H. Yu, Macromolecules 24 (1991) 2368.
[13] M. Hogan, N. Dattagupta, D.M. Crothers, Proc. Natl. Acad. Sci. USA 75 (1978) 195.
[14] J.G. Elias, D. Eden, Macromolecules 14 (1981) 410.
[15] R.J. Lewis, R. Pecora, D. Eden, Macromolecules 19 (1986) 134.
[16] D. Jary, J.-L. Sikorav, D. Lairez, Europhys. Lett. 46 (1999) 251.
[17] R.T. Kovacic, K.E. Van Holde, Biochemistry 16 (1977) 1490.
[18] H. Yamakawa, M. Fujii, Macromolecules 6 (1973) 407.
[19] T. Norisuye, M. Motowoka, H. Fujita, Macromolecules 12 (1979) 320.
[20] M.M. Tirado, C. López Martínez, J. García de la Torre, J. Chem. Phys. 81 (1984) 2047.
[21] J.M. Peterson, J. Chem. Phys. 40 (1964) 2680.
[22] Z. Dogic, A.P. Philipse, S. Fraden, J.K.G. Dhont, J. Chem. Phys. 113 (2000) 8368.
[23] P.J. Hagerman, Annu. Rev. Biophys. Biophys. Chem. 17 (1988) 265.
[24] T. Svedberg, K.O. Pedersen, The Ultracentrifuge, Oxford Univ. Press, Clarendon, 1940.
[25] R.T. Kovacic, K.E. Van Holde, Biochemistry 16 (1977) 1490.
[26] J.A. Schellman, Biopolymers 16 (1977) 1415.
[27] H. Yamakawa, M. Fujii, Macromolecules 7 (1974) 128.
[28] O. Kratky, G. Porod, Recl. Trav. Chim. Pays-Bas 68 (1949) 1106.
[29] M. Hogan, J. Wang, R.H. Austin, in: Mobility and Function in Proteins and Nucleic Acids: Ciba Foundation Symposium 93, Pitman, London, 1982.
[30] A.P. Philipse, Curr. Opin. Colloid Interface Sci. 2 (1997) 200.
[31] G.K. Batchelor, J. Fluid Mech. 52 (1972) 245.
[32] R.J. Goldberg, J. Phys. Chem. 57 (1953) 194.
[33] D.R. Lide (Ed.), Handbook of Chemistry and Physics, CRC Press, Boca Raton, FL, 1995.
[34] H. Benoit, P. Doty, J. Phys. Chem. 57 (1953) 958.
[35] J.-L. Viovy, Rev. Mod. Phys. 72 (2000) 813.
[36] L. Onsager, Ann. N.Y. Acad. Sci. 51 (1949) 627.